Impact of Radar Tilt and Ground Clutter on Wind Measurements in Clear Air

WILLIAM J. MARTIN AND ALAN SHAPIRO

Center for Analysis and Prediction of Storms, University of Oklahoma, Norman, Oklahoma

(Manuscript received 29 June 2004, in final form 29 November 2004)

ABSTRACT

From geometrical considerations, the optimum tilt angle for a meteorological radar at which the best possible vertical resolution results is derived. This optimum angle is a compromise between the effects of beam divergence and range gate spacing. For typical S-band radar parameters, this optimum tilt angle is found to be about 7°. However, wind analyses at this tilt angle were found not to be accurate in practice because of ground clutter contamination, and suboptimal angles need to be used. Most of the ground clutter was found to be sensed in the radar beam sidelobes. The data presented here imply that ground clutter is a serious contaminant at tilt angles as high as 45°. For clear-air wind profiling in the boundary layer, the impact of ground clutter contamination increased as the tilt angle was increased.

Data presented from four radars [the Goodland, Kansas, Weather Surveillance Radar-1988 Doppler (WSR-88D); the University of Oklahoma's Doppler on Wheels; NCAR's S-band dual-polarization Doppler radar (S-Pol); and NSSL's Cimarron] suggest that a fairly narrow range of tilt angles from 1° to 2° is generally acceptable for wind profiling of the boundary layer in clear-air conditions. Tilt angles outside this range lead to significant systematic errors, primarily from ground clutter contamination.

1. Introduction

This paper examines how to obtain the best wind profile from radar data and how to minimize the systematic problem of ground clutter. Radar data are widely used in the meteorological community for research and for the initialization of forecast models. Radar velocity measurements from the Weather Surveillance Radar-1988 Doppler (WSR-88D) radars of the Next-Generation Weather Radar (NEXRAD) program (Klazura and Imy 1993) are available nationwide to a 1 m s^{-1} resolution every 250 m in range from each radar. However, any systematic velocity errors, such as those caused by ground clutter, make these data potentially less valuable or even damaging for analysis and prediction.

A basic tool used in this paper is the well-known velocity–azimuth display (VAD) technique (Lhermitte and Atlas 1961; Browning and Wexler 1968). In this technique, the horizontal velocity vector is determined from a single radar measuring the radial wind speed, V_r, during an azimuthal scan. By using the following relation for the variation of measured V_r with azimuth

$$V_r = U\cos\varphi + V\sin\varphi,$$

where U and V are the components of the wind vector projected onto the radar radial (the actual horizontal wind components times the cosine of the tilt angle) and φ is the radar azimuth angle, the values of U and V can be easily found given the measured variation of V_r with φ. This relation assumes that the wind field is horizontally and temporally homogeneous, conditions most often met in meteorologically quiescent, clear-air conditions. A vertical profile of the horizontal wind vector can be obtained from a single 360° (or less) azimuthal radar scan as each range gate distance from the radar corresponds to a different height above the ground. Though this paper relies heavily on VAD analysis, the conclusions are generally valid for wind measurements under inhomogeneous conditions.

The effective vertical resolution of a wind profile that can be achieved using the VAD method depends on the radar elevation (tilt) angle. For example, if the radar has a 100-m gate spacing at a tilt of 0.5° (and a matching 200-m pulse width), then the VAD technique can give a wind vector measurement at every gate, which is every 100 $\sin(0.5°) = 0.9$ m in the vertical. This resolution is deceptive, however, as the beamwidth in the vertical

Corresponding author address: Dr. William Martin, Center for Analysis and Prediction of Storms, 100 East Boyd, SEC Room 1110, Norman, OK 73019.
E-mail: wjmartin@ou.edu

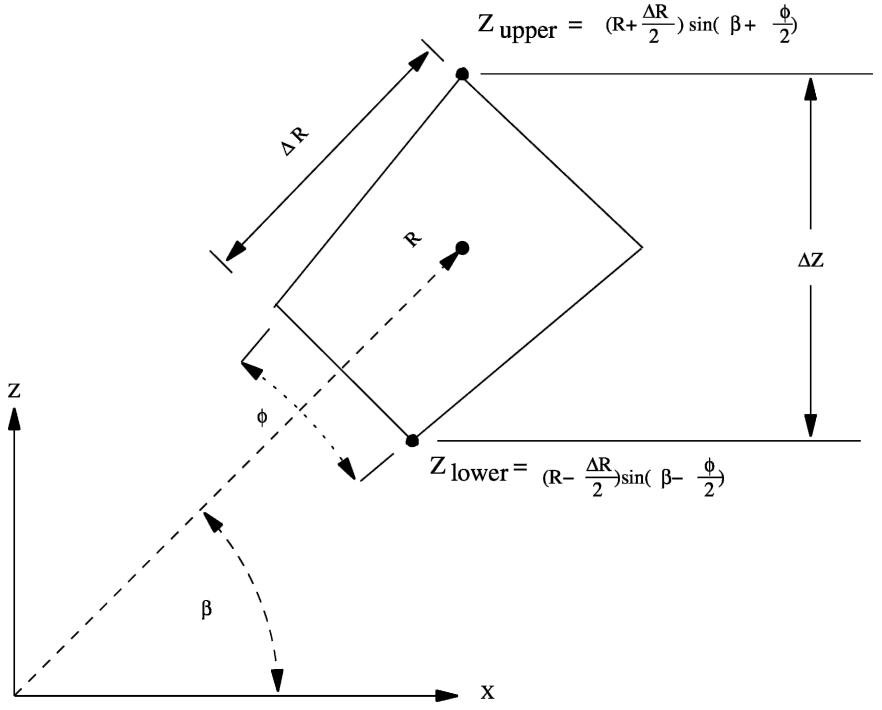

FIG. 1. Radar probe volume schematic for determining ΔZ.

is generally larger than 0.9 m. For a beamwidth of 1°, the beamwidth in the vertical at a range, R, of 57 km (corresponding to a 500-m height above the surface for a 0.5° tilt angle) would be about $2R\tan(0.5°)$, or 1000 m.

The optimal tilt angle for the best vertical resolution of a VAD-determined wind profile is achieved as a compromise between two effects: the gate spacing effect and the beamwidth effect. From practical experience, to be presented in this paper, we have found that this compromise must be significantly modified to account for the problem of ground clutter, a problem that gets worse as the elevation angle is increased. It is the purpose of this paper to analyze in some detail this issue from a theoretical and practical viewpoint.

2. Theory for optimal tilt angle

To arrive at an expression for the vertical resolution of a radar probe volume that includes effects of both beam broadening and gate spacing, consider the radar probe volume drawn in Fig. 1. If we consider ΔZ as the distance between the top and bottom points of the probe, then

$$\Delta Z = \left(R + \frac{\Delta R}{2}\right)\sin\left(\beta + \frac{\phi}{2}\right) - \left(R - \frac{\Delta R}{2}\right)\sin\left(\beta - \frac{\phi}{2}\right), \quad (1)$$

where ΔR is the gate spacing (typically half the pulse length), R is the slant range, β is the tilt angle, and ϕ is the beamwidth.

After simplification, (1) becomes

$$\Delta Z = 2R\cos\beta\sin\frac{\phi}{2} + \Delta R\sin\beta\cos\frac{\phi}{2}. \quad (2)$$

Using $R = Z/\sin\beta$ and setting $(\partial\Delta Z/\partial\beta) = 0$ (for constant Z) results in the following relation for β_{opt}, the tilt angle that will minimize ΔZ:

$$\frac{1}{2}\sin 2\beta_{\text{opt}}\sin\beta_{\text{opt}} = \frac{2Z}{\Delta R}\tan\frac{\phi}{2}. \quad (3)$$

This is equivalent to the cubic equation

$$\cos^3\beta_{\text{opt}} - \cos\beta_{\text{opt}} + \frac{2Z}{\Delta R}\tan\frac{\phi}{2} = 0. \quad (4)$$

This equation is most easily solved by iteration for β_{opt}. Figure 2 plots this optimum tilt angle versus height above the ground for WSR-88D beamwidth and gate spacing.

Since it is not convenient to use a different radar tilt angle for every layer of the wind profile desired, a decision needs to be made as to the level in which the best

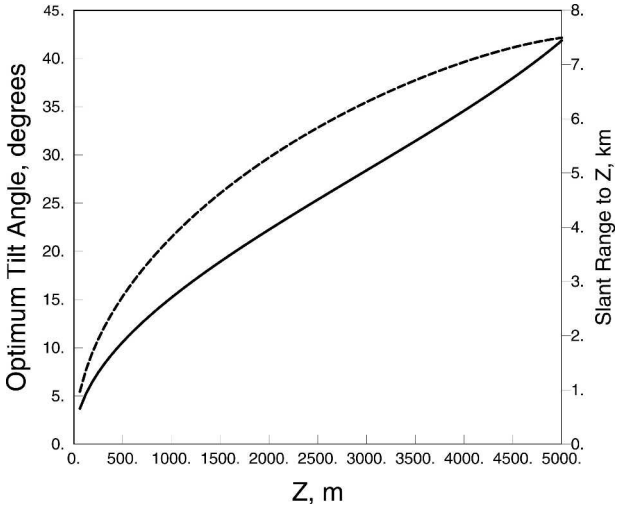

FIG. 2. Optimum tilt angle, β_{opt}, as a function of height above the ground (solid line). Dashed line is the radar slant range required to reach the height using angles from (4). Plot is for a WSR-88D radar with a beamwidth ϕ of 0.95° and a gate spacing of 250 m.

resolution is desired. For the example of the low-level jet (LLJ) examined in section 3, the elevation that requires the best resolution is the lower shear layer, where the wind profile most rapidly changes with height. This is typically from the surface to 500 m. If we decide to put the best resolution at 250 m above the ground, Fig. 2 then suggests that a tilt angle of about 7° would be desirable in terms of obtaining the best vertical resolution of that layer when using a WSR-88D radar. The vertical resolution would then be about 60 m [from (2)]. Table 1 shows the calculated optimal tilt angles and resulting vertical resolution for five radar configurations (with data to be examined in sections 3 and 6).

It is worth noting that using a high tilt angle of 7°–10° has other advantages in addition to improving the vertical resolution. High tilts greatly reduce problems from beam refraction through refractive index gradients (including anomalous propagation), and obtain the VAD wind profile over a much smaller scan radius so that the VAD assumption of horizontal homogeneity is more likely to be valid.

In the next section, it is shown that these theoretical results need substantial modification in order to deal with the practical problem of ground clutter.

TABLE 1. Optimal tilt angle and resulting vertical resolution at a level 250 m above the surface for five radar configurations.

Radar	Beamwidth (°)	Gate spacing (m)	β_{opt} from (4) (°)	ΔZ from (2) (m)
Cimarron	0.90	150	9.38	48.2
WSR-88D	0.95	250	7.43	64.1
DOW3	0.93	137	9.99	46.8
DOW3	0.93	12	42.7	12.5
S-Pol	0.91	149	9.46	48.3

3. VAD-determined wind profiles as a function of radar elevation angle

In this section, wind profiles obtained by the VAD technique using the KGLD WSR-88D radar and the Doppler on Wheels (DOW3) radar located in Goodland, Kansas, are considered. Wind profiles obtained from two other radars are discussed in section 6.

The DOW3 radar (Wurman et al. 1997) was collocated with the KGLD WSR-88D at Goodland on the night of 30 May 2000. DOW3 was less than 50 m due north of the KGLD tower. Radar scans appropriate for VAD analysis were obtained at approximately 0600 UTC from both radars. The amplitude of the low-level jet at this time was about 30 m s^{-1}. Since the Nyquist speeds for KGLD and DOW3 were, respectively, 26 and 16 m s^{-1}, significant aliasing of the radial velocity measurements occurred. The dealiasing algorithm applied to the data was specifically designed for clear-air VAD data. Details of this algorithm and of the procedures used in the VAD analysis can be found in Martin (2003, chapter 4).

There are a number of generally equivalent ways to obtain the horizontal wind vector using the well-known VAD technique. For the data analyzed in this paper, a least squares best-fit sine wave technique was used. In this method, the components of the horizontal wind vector are varied until the total squared error between the measured radial velocity and the VAD model is minimized. Specifically, the cost function, J, defined as

$$J = \sum (V_r - U\cos\varphi - V\sin\varphi)^2,$$

is minimized. The summation is taken over all the points along a complete azimuthal circle and at one range gate. For WSR-88D data, this is typically about 360 data points, with one V_r measurement per degree. One fit for U and V gives the horizontal wind vector at one height (viz., $Z = R\sin\beta$). Wind profiles are obtained by doing a VAD analysis of the data obtained from each range gate. For quality control, an attempt was made to filter out V_r data that might have been contaminated by ground clutter. Three quality-control tests were applied: Only data with reflectivities between −20 and 50 dBZ, data with V_r absolute values greater than 3 m s^{-1}, and data with spectral width values less than 7 m s^{-1}, were included in the analysis. The

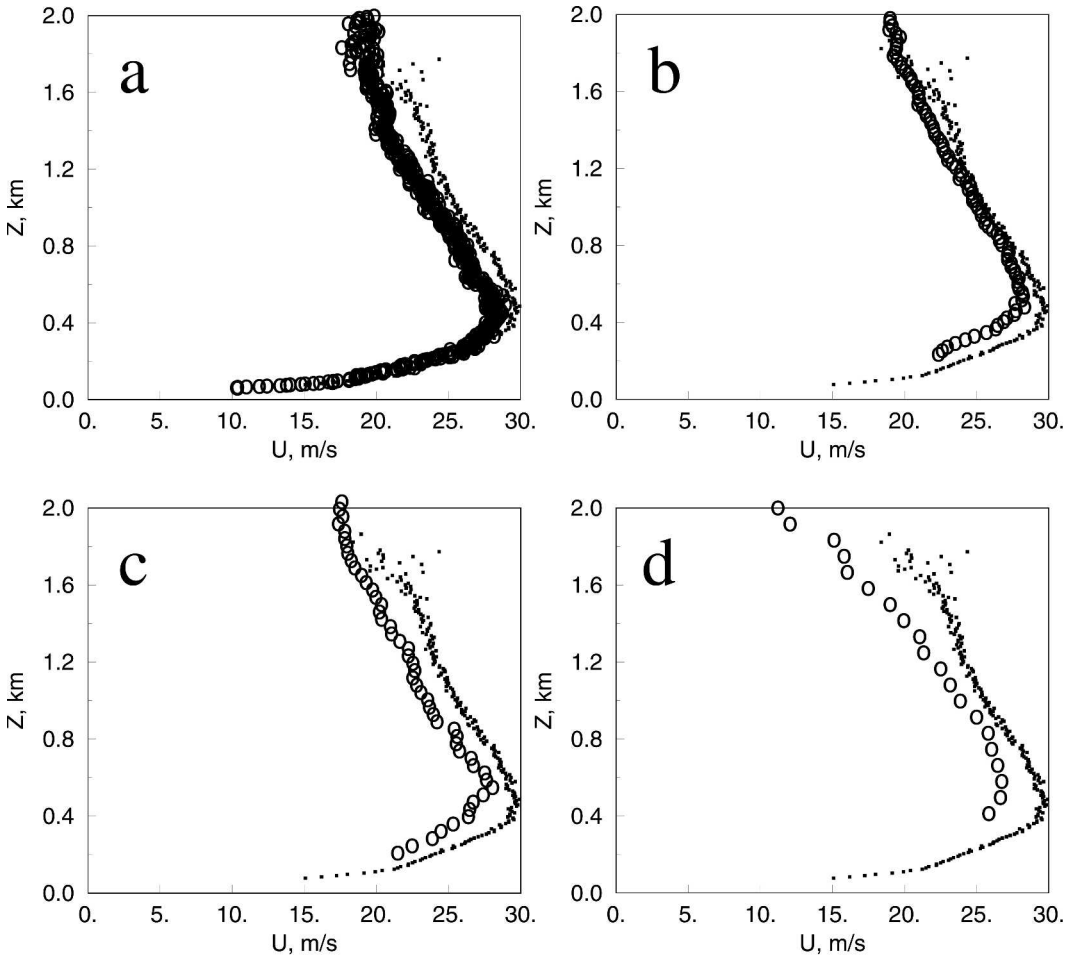

FIG. 3. Wind speed profiles from VAD analysis of KGLD WSR-88D data from near 0600 UTC 30 May 2000 at four elevation angles. Profiles are plotted as open circles at tilt angles of (a) 0.5°, (b) 4.5°, (c) 8.5°, and (d) 20°. Plotted dots on each subfigure represent the 1.5° elevation KGLD wind profile from the same volume scan for reference.

computed values of height above ground (Z values) were corrected to take into account the earth's curvature and the standard atmosphere refractive index by assuming the earth's radius to be $4/3R_{\text{earth}}$ (Battan 1973, p. 24). This correction was found to be important at the lower tilt angles. Finally, the determined best-fit wind vector was divided by the cosine of the elevation angle to account for the fact that, due to the radar tilt angle, the radar does not sense the full horizontal wind speed. This last correction is very minor, even at tilt angles of 20°.

Figure 3 displays the VAD-determined wind speed profiles obtained from the KGLD radar from tilt angles 0.5°, 4.5°, 8.5°, and 20°. Though the conditions at the time were clear air, this radar was in precipitation mode using Volume Coverage Pattern 11 (VCP 11; OFCM 1991). As discussed later, the 1.5° tilt wind profile is probably the most accurate and has been plotted in each subfigure of Fig. 3 for reference. Figure 4 shows the analogous profiles from DOW3 at approximately the same tilt angles along with the same 1.5° KGLD reference profile. The data from KGLD were obtained from 0546 to 0550 UTC, and the data from DOW3 were obtained from 0555 to 0559 UTC. Consequently, there is a 10-min time difference between the KGLD and DOW3 wind profiles. Other than this small time difference, the two sets of wind profiles were obtained from measurements of air at nearly the same locations and times. Ideally, all the wind profiles shown in Figs. 3 and 4 would be identical; however, some tilt-dependent effects are clearly evident. Consulting Table 1, the theoretically best tilt angles for KGLD and DOW3 are 7° and 10°, respectively; however, the 1.5° KGLD profile appears to have the least noise and the most vertical detail.

Figure 4a indicates a particularly serious problem for DOW3 at 0.5° tilt. The reduced height of the profile

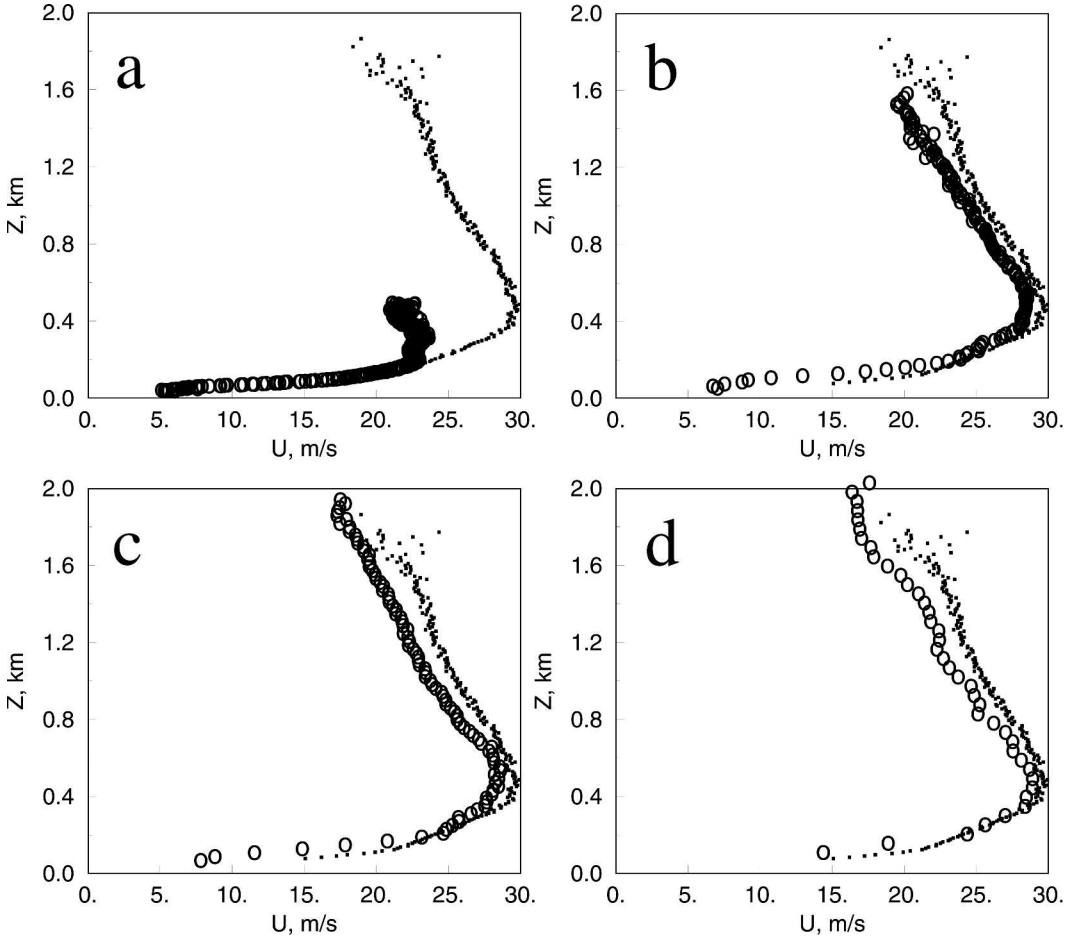

FIG. 4. Same as Fig. 3 but from DOW3 radar with 1.5° KGLD profile plotted for reference.

obtained from DOW3 at this elevation is simply caused by the limited range of the beam. The distortion of the velocity peak is possibly caused by inhomogeneous refractive index gradients leading to inaccurate beam placement in the vertical. Beam bending is most significantly a problem at low tilt angles (Battan 1973, 17–28). The underestimation of the winds at the 0.5° tilt for DOW3 could be caused by an unusually high level of ground clutter contamination at this low tilt angle. The absence of this problem in the KGLD data of Fig. 3a may be due to the fact that, while the DOW3 antenna was 3 m above the surface, the KGLD antenna is on top of a tower with a feed horn 20 m above the surface.

Both radars show a degradation of the accuracy of the wind profile relative to the reference profile as tilt angle is increased, with the problem being worse for KGLD. In all cases, wind measurements are underestimated at tilts both below and above 1.5°. The underestimation is typically a few meters per second. While the underestimation tends to be larger at the higher tilt angles, it is largest for the lowest-tilt DOW3 data, reaching 7 m s^{-1}. Larger errors were found for the S-band dual-polarization Doppler radar (S-Pol) and the Cimarron radar discussed in section 6.

Ideally, with a horizontally homogeneous wind field, the wind profiles determined by VAD analysis would be independent of the elevation angle used, with the only difference being the number of points in the vertical where independent measurements were obtained, and the effective resolution of those measurements. In view of the results from section 2, it was expected that radar tilt angles of about 7°–10° would be best, but this is not the case for the data considered herein. The reason the tilt angle affects the wind profile in unanticipated ways can be appreciated by considering the plan position indicator (PPI) velocity scans of the same data used to extract the wind profiles of Figs. 3 and 4. Figure 5 shows PPI velocity scans for the KGLD radar, and Fig. 6 shows the corresponding scans from DOW3. To facilitate comparison, Figs. 5 and 6 are plotted with the same spatial scales and with the same grayscale table. Also, these figures use height above the ground as the

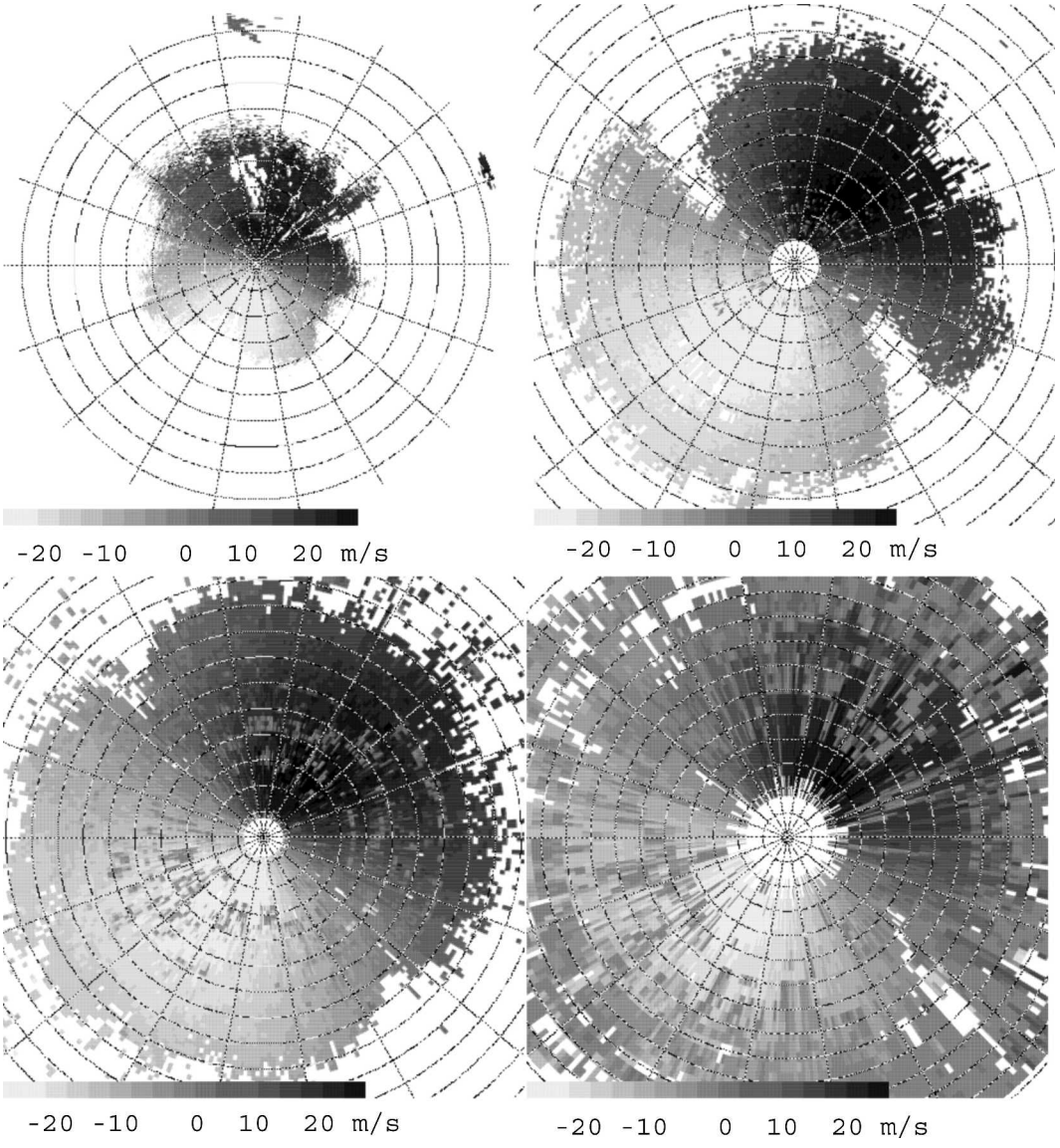

FIG. 5. PPI radial velocity scans from KGLD corresponding to profiles shown in Fig. 3. Upper left is for 0.5° of tilt, upper right is for 4.5°, lower left is for 8.5°, and lower right is for 20°. Range rings are drawn at radial intervals corresponding to vertical heights every 200 m above the ground. The actual ranges are approximately (200 m)/sinβ per range ring. Grayscale for speed magnitude ranges from -25 (very light gray) to 25 m s^{-1} (black).

radial distance, rather than distance along the beam (i.e., the range rings drawn are scaled to height above the ground, with a ring drawn every 200 m above the ground). This makes the comparison of the PPI velocity plots with the derived profiles of Figs. 3 and 4 much easier, and also makes it easier to compare PPI plots at different tilts.

These figures display data only where the received radar signal was above the noise level (and for KGLD, where second trip contamination was not detected). The shape of the displayed data is ordinarily expected to be circular if the flow is horizontally homogeneous with an even distribution of scatterers to a certain depth [probably insects for this case (Wilson et al. 1994; Martin 2003, chapter 3)]. This circular pattern is plainly evident at the higher tilt angles; however, at 0.5° tilt (Fig. 5, upper left for KGLD), a noncircular pattern is seen. The probable reason for this distortion is that the beam has been bent by vertical gradients in the refractive index. Small horizontal gradients in the refractive index can result in horizontally inhomogeneous beam propagation and noncircular signal patterns at low tilt angles, such as the one seen in Fig. 5 (upper left). Since the refractive index profile is a thermodynamic prop-

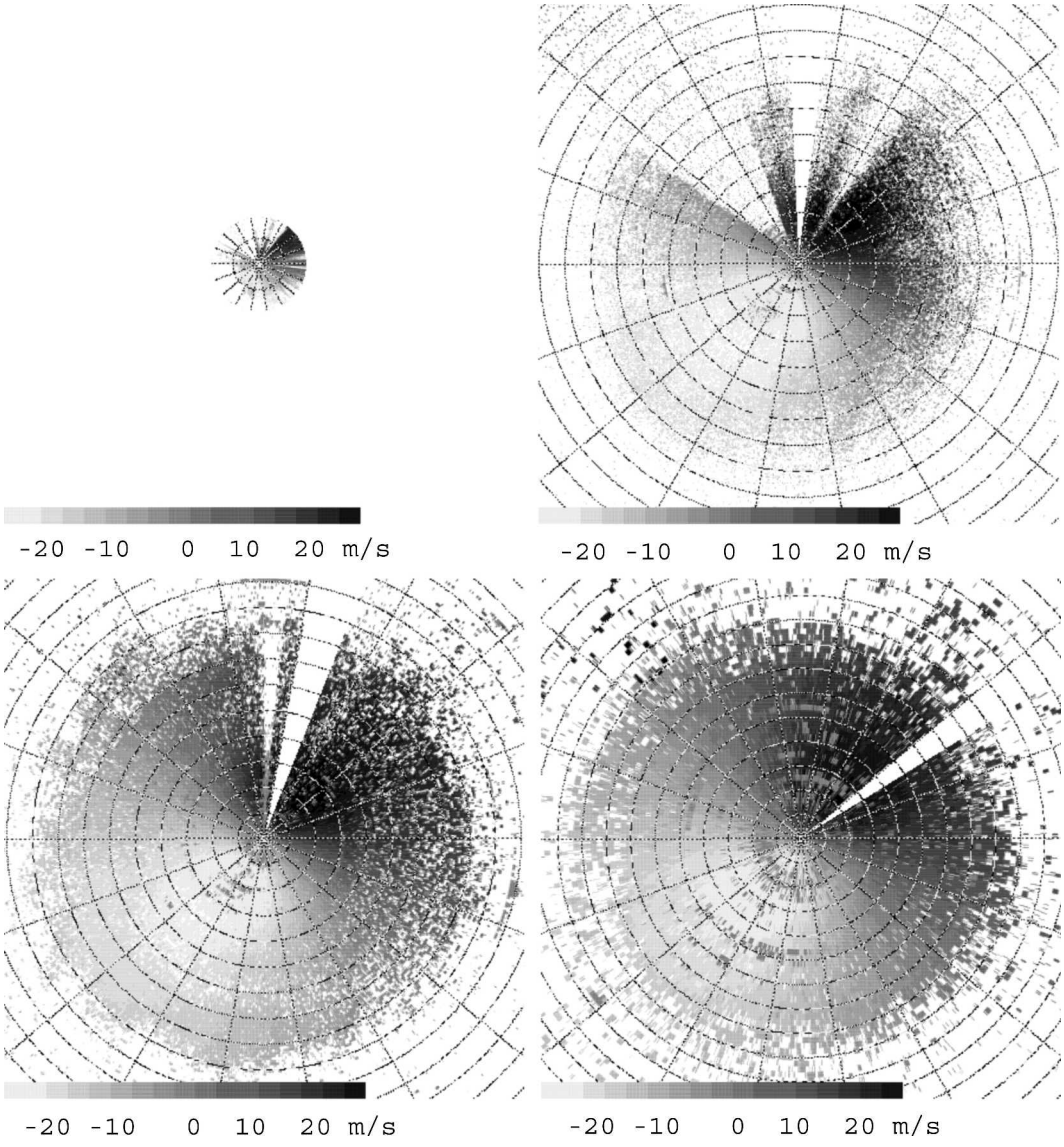

FIG. 6. PPI velocity scans from DOW3 corresponding to profiles shown in Fig. 4. Upper left is for 0.5° of tilt, upper right is for 4.5°, lower left is for 8.5°, and lower right is for 20°. Range rings are drawn at radial intervals corresponding to vertical heights every 200 m above the ground. Grayscale for speed magnitude ranges from −25 (very light gray) to 25 m s^{-1} (black).

erty, it is not directly known from radar data alone. Knowledge of the refractive index gradient in the vertical and horizontal sufficient for correcting this problem by beam tracing would be difficult to obtain. High-resolution numerical weather prediction (NWP) model data could potentially provide a precise refractive index distribution, provided the model physics were accurate enough, but this has not been explored here.

Evidence of ground clutter contamination of the radial velocity measurements, a problem that gets worse at higher tilt angles, can be seen in Figs. 5 and 6. Since the ground has no velocity, ground clutter presents as zero velocity (medium gray in these PPI scans). Ground clutter contamination is obvious in the plots as spots of a few gray pixels in the middle of the high-speed regions (black or white). The spiral pattern of missing data (white) in the upper-right panel of Fig. 5 is caused by the clutter filter employed by the KGLD radar. WSR-88Ds have available a variety of complex clutter filter algorithms, which are selectable by the operator. Clutter filter information is not saved in the WSR-88D level II data format, so it is not possible to discern what clutter filter algorithm was used for these particular data, or any archived level II WSR-88D data. WSR-

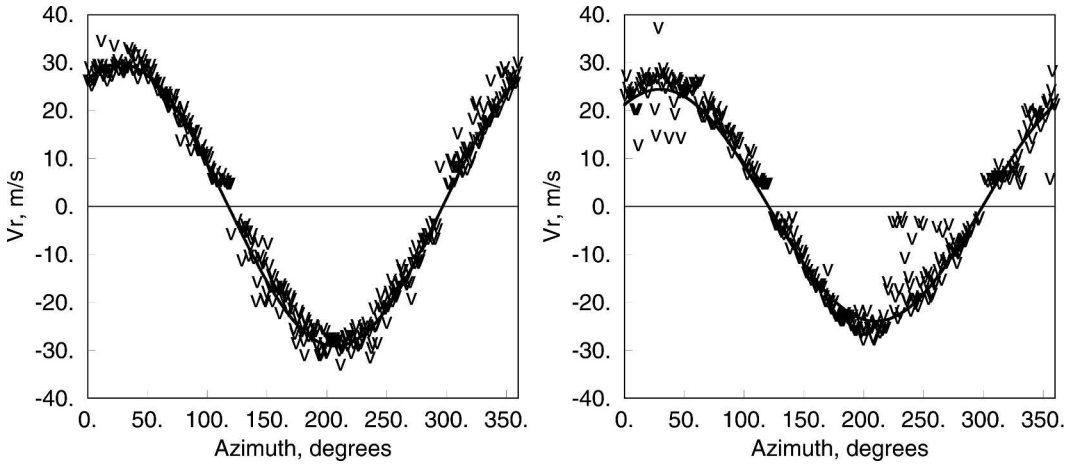

FIG. 7. VAD at a range of 400 m above the ground from KGLD radar. (left) 1.5° tilt; (right) 8.5° tilt. The v's are the raw (though dealiased) radial velocity data, and the solid curve is the best-fit sine wave.

88D clutter filter algorithms involve the usage of a known ground clutter map and attempt to correct reflectivity values. Data of zero radial velocity were not used in the VAD analyses presented here; these values were filtered out because of the possibility that they might be contaminated by ground clutter. Data from pixels in Figs. 5 and 6 that are obvious ground clutter were not used in determining the wind profiles in Figs. 3 and 4. However, ground clutter contamination can be more subtle. Radars determine the velocity from a number of pulses, which are combined to produce a velocity spectrum. The first moment of the velocity spectrum is the radial velocity. Ground clutter affects the spectrum by adding a peak near zero speed. For strong ground echoes, most of the signal is ground clutter, and a zero velocity measurement results. However, if the ground clutter is weak (but still present), its zero speed is not weighted heavily. The result is a velocity measurement that is not zero but biased low. An erroneous low measurement of the velocity caused by ground clutter contamination is the most likely explanation for the poor wind profiles at higher radar tilt angles seen in Figs. 3 and 4. This is further supported by Fig. 7, which shows the data used in the VAD analyses for the vertical location in the wind profile 400 m above the surface, at 1.5° and 8.5° tilts by KGLD, along with the best-fit solution curves for the wind. The 8.5° VAD has numerous low-speed data below the solution curve that the 1.5° VAD does not have. These low-speed data are very likely erroneous in value due to ground clutter contamination of the velocity spectrum. Even if these low velocity points could somehow be filtered out, the envelope of what appear to be good data still has a smaller amplitude at 8.5° than at 1.5°, and it may well be that most of the data points in the 8.5° VAD were derived from velocity spectra contaminated to some extent by ground clutter.

A sample of reflectivity PPI scans from KGLD and DOW3 is shown in Fig. 8. Both of these reflectivity scans are plotted on identical spatial scales and use the same grayscale table to display reflectivity intensity. They correspond to the 8.5° velocity PPI scans in Figs. 5 and 6. The better spatial resolution of DOW3 relative to KGLD is apparent (137-m gate spacing versus 1000 m). Also, while DOW3 has measured reflectivity in the same air and at nearly the same time as KGLD, KGLD has measured a higher reflectivity. This is because DOW3 has a 3-cm wavelength, versus 10 cm for WSR-88D. The scattering targets in this case were probably insects (Wilson et al. 1994; Martin 2003, chapter 3), and 10-cm radars are more sensitive than 3-cm radars to targets the size of typical insects. Little ground clutter is apparent in Fig. 8. KGLD, of course, has been ground clutter filtered, but DOW3 has not. Many locations with obvious ground clutter in the velocity scan in the lower left of Fig. 5 do not correspond to high reflectivities in the dBZ scan of Fig. 8. Nonetheless, ground clutter contamination is still present, even if the reflectivity of the ground is too weak to stand out in the reflectivity display. Ground clutter is a larger problem for clear-air radar data such as these, due to the very weak clear-air reflectivity (relative to precipitation). Even very weak signals from sidelobes can contaminate the signal, if the meteorological signal is weak.

4. Sidelobes and sidelobe screening

We have found the problem of ground clutter contamination to be worse at higher tilt angles. Why this is so can be answered by referring to the range–height

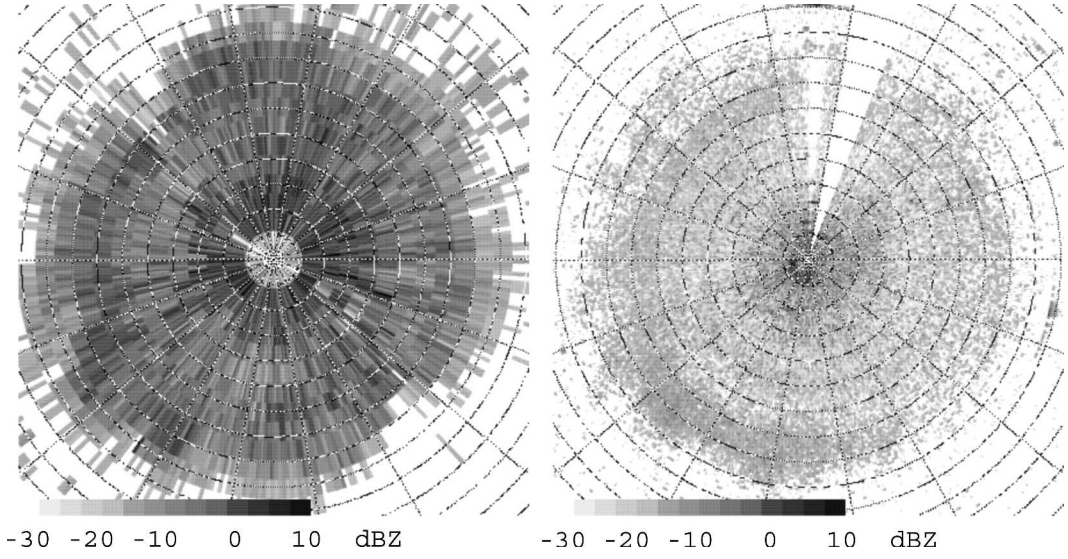

FIG. 8. Reflectivity PPI scans from (left) KGLD and (right) DOW3. Both are at about 8.5° tilt, were acquired at the same time and location, and have the same grayscale intensity map. Reflectivity scale varies linearly from −30 (white) to 10 dBZ (black).

indicator (RHI) reflectivity and velocity scan shown in Fig. 9. For this scan, DOW3 was operated at the maximum possible resolution setting of 12-m gates, in the same location and at approximately the same time that the PPI scans for the VAD analyses for Fig. 4 were obtained. The point targets evident in the reflectivity scan are believed to be insects, and account for most of the received signal. These targets are present up to a height of about 2 km. Ground clutter is also apparent in the reflectivity and velocity scans, especially between 0.8 and 1.6 km of slant range from the radar (the sector of high reflectivity from 0 to 0.4 km of range is due to

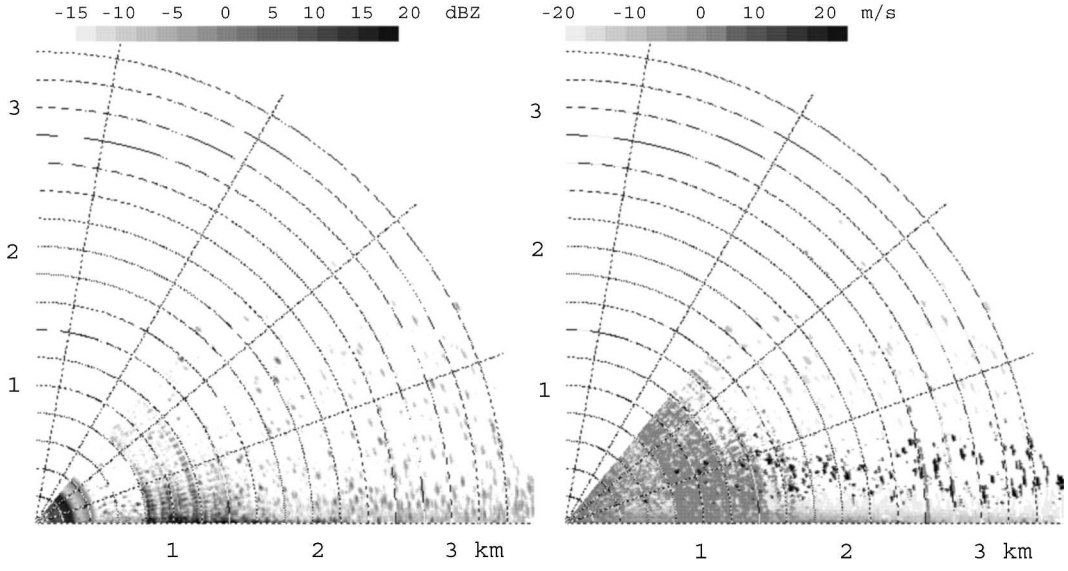

FIG. 9. (left) RHI reflectivity scan from DOW3 radar at Goodland, KS, at 0548 UTC 30 May 2000. The radar was pointing along azimuth 180° (due south). Range rings are 200 m apart. Radials are drawn every 20°. Significant clutter is seen at a range of 0.8–1.6 km at all tilt angles. Internal electronic interference causes spurious signal at ranges less than 0.4 km. (right) RHI velocity scan at the same time. Ground clutter appears as a uniform medium gray (zero velocity). Reflectivity grayscale (top of figure) varies from −15 (white) to 20 dBZ (black), and velocity grayscale varies from −20 (very light gray) to 20 m s^{-1} (black).

electronic interference). Clutter appears as arcs of high reflectivity collocated with arcs of zero radial speed. These arc patterns indicate that ground targets are being illuminated by radar sidelobes.

DOW3 was parked just to the south of the KGLD radar tower. An open field to the south of this site (180° azimuth) extends to a range of about 1 km. Immediately south of this field is the town of Goodland. The ground clutter in Fig. 9 begins at about 0.8 km in range, which is near the northern boundary of the street network of Goodland. Beyond 1.6 km of range, the sidelobes of the radar are apparently screened out by ground targets (Doviak and Zrnić 1985) and the problem is greatly reduced. Also, note in the reflectivity scan of Fig. 9 that the sidelobe structure of the radar beam can be inferred from the modulation in signal strength with elevation at individual gates. For example, at a range of about 1.2 km, the reflectivity modulates in elevation through about 17 maxima in 40° of elevation. Each maximum corresponds to a particular sidelobe intersecting a ground target. In fact, one method of determining a beam power plot is to scan a point target of known reflectivity.

The theoretical beam pattern is related to a second-order Bessel function, and is relatively easy to calculate. Meteorological radars typically are designed to have an antenna illumination pattern that varies as $[1\text{-}(2r/D)^2]^2$, where r is the distance from the center of the antenna and D is the antenna diameter. This is done to reduce the strength of sidelobes at the expense of widening the main lobe. For this illumination pattern, the normalized beam power pattern, f^2, is (Sherman 1970)

$$f^2(\theta) = \left[\frac{8J_2(x)}{x^2}\right],$$

where

$x = \pi \mathrm{D} \sin\theta/\lambda,$

J_2 = Bessel function of the first kind of order two, and

λ = radar wavelength.

Figure 10 depicts the theoretical beam power pattern for the wavelength and antenna size of the DOW3 radar (3.198 cm and 2.44 m, respectively), and an observed beam power plot obtained from the RHI data shown in Fig. 9. For the observed power plot, the reflectivity data at a range of 1164 m are plotted as a function of the elevation angle. The 1164-m range corresponds to the range of the strongest ground target seen in Fig. 9. The theoretical beam power plot is scaled so that it matches the peak in reflectivity seen in the data. The first theoretical sidelobe is 25 dB weaker than the main lobe; however, subsequent sidelobes fall off more gradually. For off-axis angles beyond the first few sidelobes, the measured DOW3 sidelobe energy is much greater than the theoretical curve. These discrepancies are typical for radars, including the WSR-88D (OFCM 1990, 3–28), due to nonideal antenna geometry. Since clear-air radar signals are much weaker than typical signals from precipitation, ground clutter (and residual ground clutter after a clutter filter has been applied) is a larger source of contamination for clear-air data.

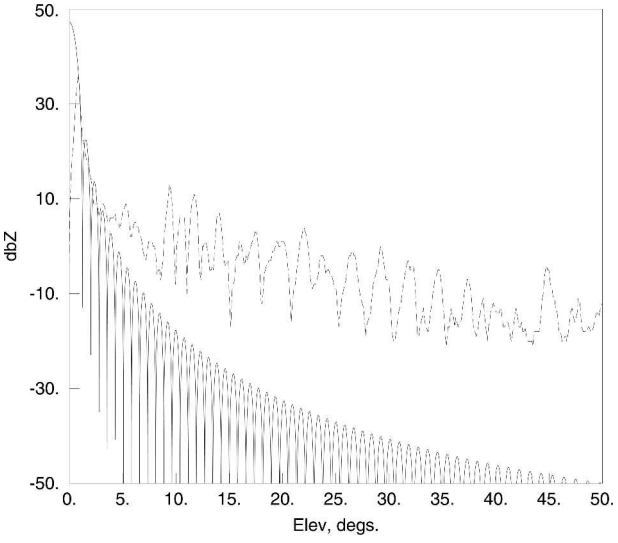

FIG. 10. DOW3 theoretical beam power plot (solid curve) and observed beam power plot determined from a strong ground target (dashed curve).

For this site, ground clutter is generally a problem at all tilt angles for gates less than about 1.6 km from the radar. When a low tilt angle is used for VAD work, most of the gates used for determining the wind profile will be beyond this distance, and the problem of ground clutter is limited to the lowest levels of the profile. However, at higher tilt angles, more radar gates used to measure the low-level wind will sample the clutter, and systematically underestimated and noisy wind measurements may result.

Assuming that, in general, ground clutter contamination falls within a hemisphere centered on the radar of some radius, R_{clutter}, a radar tilt angle can be chosen such that wind measurements above a certain minimum height, Z_{min}, will be made outside this circle. Approximately, this tilt angle is β_{clutter}:

$$\beta_{\text{clutter}} = \tan^{-1}\left(\frac{Z_{\text{min}}}{R_{\text{clutter}}}\right). \quad (5)$$

If we desire accurate winds above 200 m and (as Fig. 9 suggests) ground clutter is limited to 1.6 km from the

radar, then (5) gives a maximum tilt to use of 7°. However, the problem of ground clutter is worse for KGLD than DOW3. This is possibly because DOW3 has a smaller probe volume or (more likely) because the antenna for KGLD is atop a tower, while DOW3 was near the ground. The screening effect of sidelobes by surface targets does not occur to as great an extent for elevated antennas (Doviak and Zrnić 1985). Figures 3b and 3c show degraded wind profiles from KGLD below approximately 0.8 and 1.9 km for 4.5° and 8.5° tilts. Using these values in (9) to solve for R_{clutter} gives R_{clutter} consistently of about 11 km for both tilts. For this R_{clutter}, and a Z_{min} of 200 m, (9) gives a maximum tilt of about 1.0° to avoid problems from ground clutter. This is consistent with the KGLD wind profile obtained from the 1.5° tilt being considered the most accurate (of the available tilts) and used as the reference profile in Figs. 3 and 4.

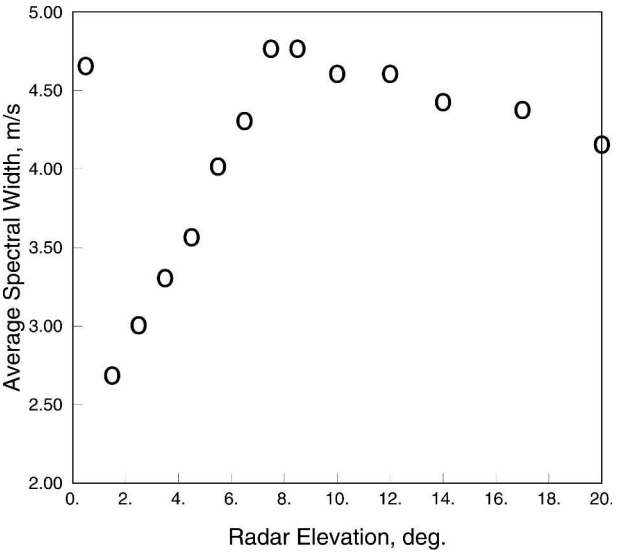

FIG. 11. Average of spectral width data below 1 km above the ground as a function of radar tilt angle. Data are from KGLD radar near 0545 UTC 30 May 2000.

5. Using spectral width information for quality control

One indication that the 1.5° tilt provides the most accurate wind profile comes from the spectral width information. Ground clutter contamination can increase the spectral width due to the combination of a spectral peak near zero speed from ground clutter with a second spectral peak near the actual wind speed. Figure 11 presents the average spectral width value below an elevation of 1 km for the KGLD radar volume scan used for Fig. 3, as a function of elevation angle. All available tilts from VCP 11 were used in Fig. 11. The minimum average spectral width occurs at an elevation angle of 1.5° and increases steadily with higher elevation angle. The spectral width is significantly higher at 0.5° than at 1.5°, possibly because part of the main lobe intersects the ground.

Because spectral width can indicate ground clutter contamination, some benefit may come from rejecting data that have large spectral widths. Figure 12 presents results for different levels of data rejection based on spectral width information. Figure 12a shows the difference between the 1.5° tilt VAD-derived reference profile and that derived from 0.5° tilt data with no spectral width filtering. Similarly, Figs. 12b, 12c, and 12d show the difference profiles when only data with a spectral width less than 7, 5, and 3 m s^{-1}, respectively, are used in the 0.5° VAD analysis. VAD analyses were unsuccessful if a spectral width threshold much below 3 m s^{-1} was used, as too much data were rejected (not shown). The difference between the two profiles is reduced as the level of data rejection is increased. The 0.5° profile using the 3 m s^{-1} spectral width threshold shows the least difference from the 1.5° profile and is, therefore, probably the most accurate. However, using a 3 m s^{-1} threshold has resulted in a rejection of 80% of the data, and the wind profile is significantly noisier. For the higher tilt profiles, no benefit was found from using spectral width information to filter the data. Even though elevated spectral widths were present at the higher tilts (as shown in Fig. 11), most of the high-spectral-width data occurred with low velocity measurements that were already filtered out by a previous step in quality control in which velocities below 3 m s^{-1} were rejected.

6. Contamination evidence from two other radars

We now present some results from two other radars, the S-Pol radar operated by the National Center for Atmospheric Research (NCAR) and the Cimarron radar operated by the National Severe Storms Laboratory (NSSL) (Zahrai and Zrnić 1993). Both of these instruments are research S-band radars. Figure 13 shows VAD wind profiles derived from S-Pol scans. Plotted are the 0.5°, 4.5°, 8.5°, and 10.5° profiles with the 2.5° profile plotted as dots on each as a reference profile (the 1.5° tilt was not available). These data were obtained with S-Pol deployed near Idalia, Colorado, near noon local time (1840 UTC) on 14 July 2000 under clear-air conditions. This radar was sited deliberately in a shallow depression in the terrain in an attempt to minimize ground clutter by way of screening of sidelobes. Nonetheless, these profiles show unmistakable

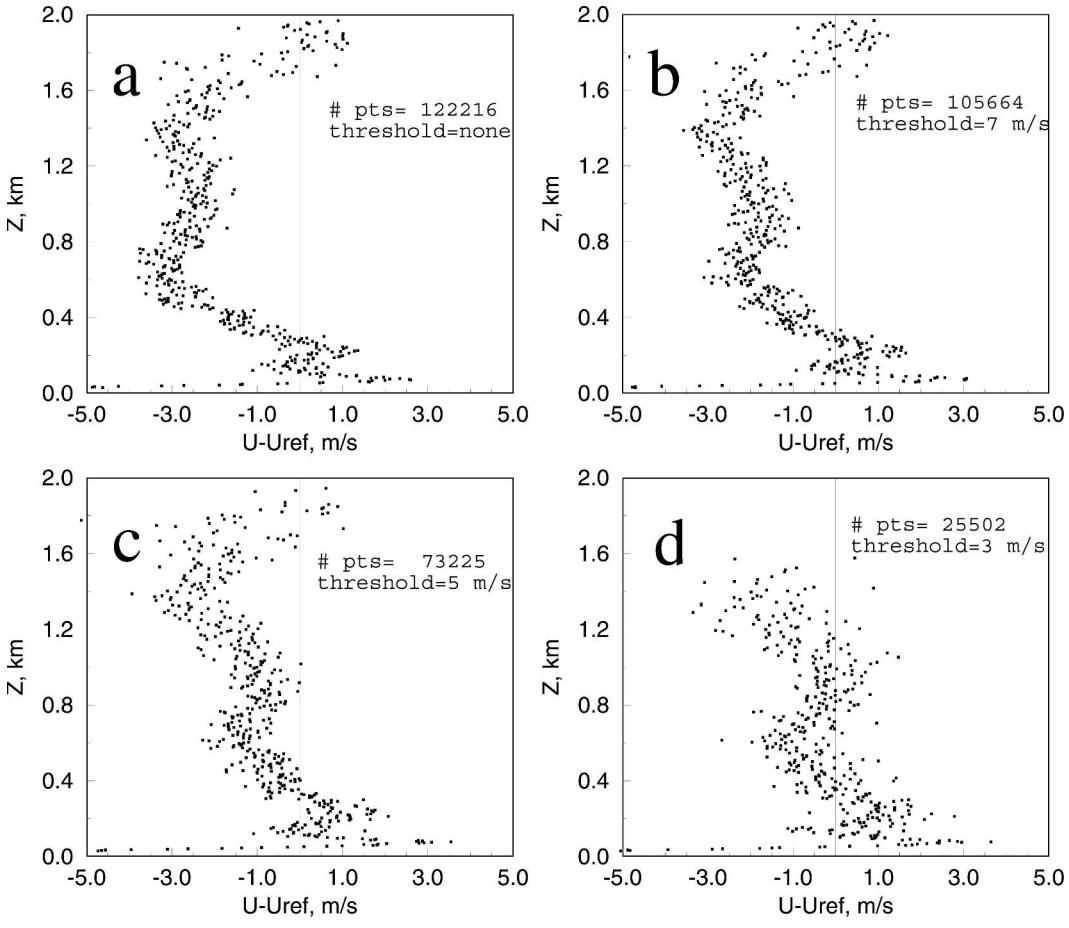

FIG. 12. Difference between 0.5° tilt wind profile and the 1.5° reference wind profile for different levels of data rejection for (a) no data rejection based on spectral width, (b) data with spectral width greater than 7 m s^{-1} rejected, (c) data with spectral width greater than 5 m s^{-1} rejected, and (d) data with spectral width greater than 3 m s^{-1} rejected. Also indicated on each plot is the number of data points that passed through quality control.

degradation of the wind profiles due to ground clutter contamination. Figures 13b, 13c, and 13d show significant noise in the profiles and underestimation of the wind below 0.55, 1.0, and 1.2 km, respectively. From (9), this leads to a consistent $R_{clutter}$ of about 7 km.

Figure 14 shows VAD wind profiles for a low-level jet obtained with the Cimarron radar at 0700 UTC 16 June 2000, with similar problems. Presented are profiles obtained from tilt angles 4.0°, 8.0°, 10.0°, and 16.0° in Figs. 14a, 14b, 14c, and 14d. Each figure has the 2.0° profile plotted as the reference profile. This figure shows errors in velocity measurements exceeding 10 m s^{-1}. The degradation of the wind profile at higher tilt angles in Fig. 14 implies an $R_{clutter}$ of about 7.5 km.

7. Summary and conclusions

This paper derives theoretically the best radar tilt angle, β_{opt}, to use for maximizing the vertical resolution of VAD-derived wind profiles. This angle is a compromise between gate spacing and beamwidth effects. The value is given implicitly by (4). For boundary layer wind measurements, these formulas give a best tilt angle for typical S- and X-band radar configurations of 7°–10° and a best obtainable vertical resolution of about 50 m. However, from practical experience, we have found that the selection of tilt angle needs to be amended by considering the amount of ground clutter contamination. For the cases considered herein, ground clutter was observed to be a problem at all tilt angles, but only for distances within a distance $R_{clutter}$, which is likely related to the screening of sidelobe energy by ground targets. This leads to the need to have

$$\beta_{clutter} < \tan^{-1}\left(\frac{Z_{min}}{R_{clutter}}\right),$$

where Z_{min} is the level above which winds are desired and $R_{clutter}$ is the distance from the radar at which

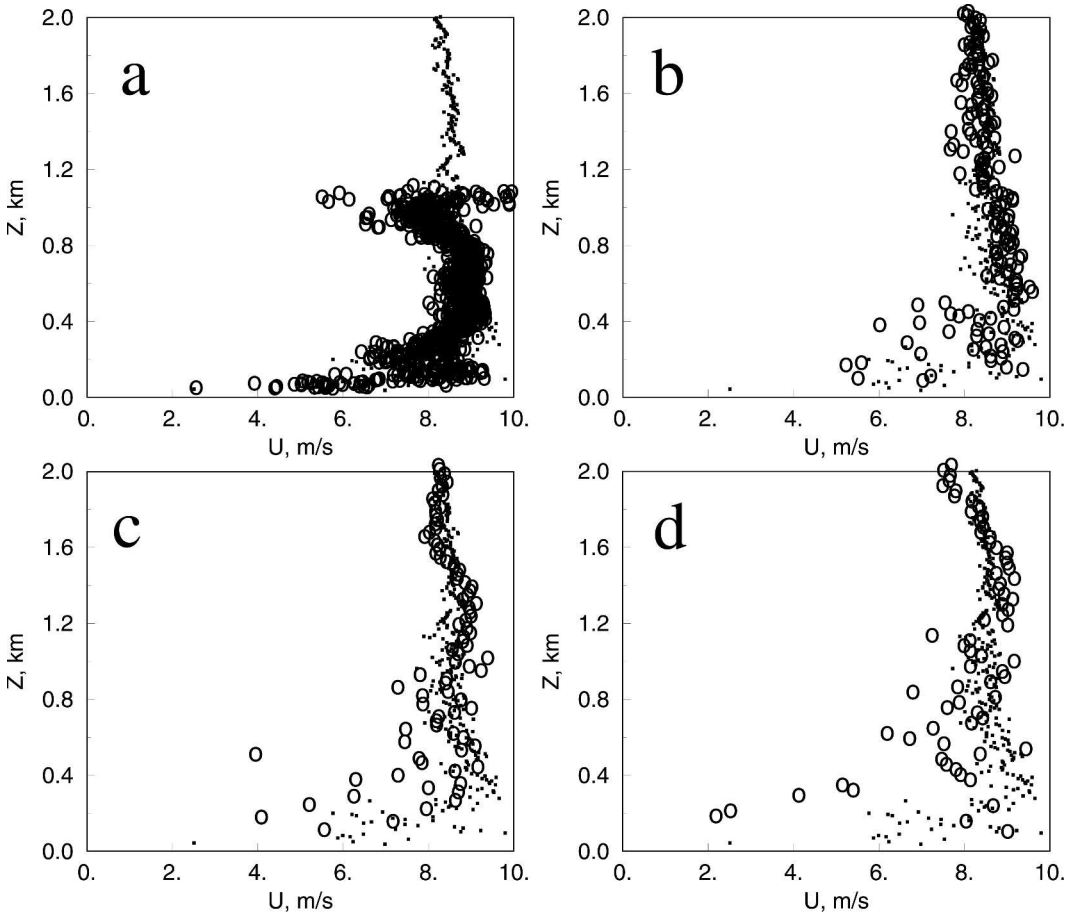

FIG. 13. Daytime VAD wind profiles from S-Pol radar on 14 Jul 2000 for tilt angles of (a) 0.5°, (b) 4.5°, (c) 8.5°, and (d) 10.5°. Wind profiles are plotted as open circles, and each figure has a reference profile plotted as dots. The reference profile is the VAD profile obtained at 2.5° tilt.

ground clutter is a problem. Ground clutter is a larger problem for clear-air radar data than for radar data of precipitation targets because clear-air targets are typically much weaker, which increases the contamination of the data by ground targets in the radar sidelobes. Also, tilt angles below the beamwidth ϕ should be avoided because the intersection of the main beam lobe with the ground causes a great deal of ground clutter contamination. So we also need

$$\beta > \phi.$$

The resulting vertical resolution is then found from (2).

The main limiting factor was found empirically to be R_{clutter}. It was shown that, for VAD work with clear-air data, the problem of ground clutter gets worse as the tilt angle is increased. This is because, for higher tilt angles, data closer to the radar must be used to obtain a VAD at a particular height above the ground. Ground clutter contaminates velocity measurements at all tilt angles by way of beam sidelobes and tends to be restricted to ranges less than R_{clutter} from the radar. Since the amount of ground clutter depends on the radar and the radar site, R_{clutter} will generally be site specific. For KGLD, it was found that the 1.5° tilt produced the most accurate wind profiles. Using (2), the vertical resolution for this tilt at $Z = 250$ m is about 165 m, much less than the 64 m that would have been obtained at a tilt angle of 7° if clutter had not been a problem.

The problem of clutter contamination is radar and site specific, and it is difficult to make general statements of the severity of the problem from evidence from only four radars. However, it is important to be aware of this potential problem. For the data that we examined, we found typical errors of a few meters per second, with less common errors as large as 10 m s^{-1}. All four of the radars examined exhibited both systematic velocity errors and an increase in noise when measurements were made in ground clutter. These errors

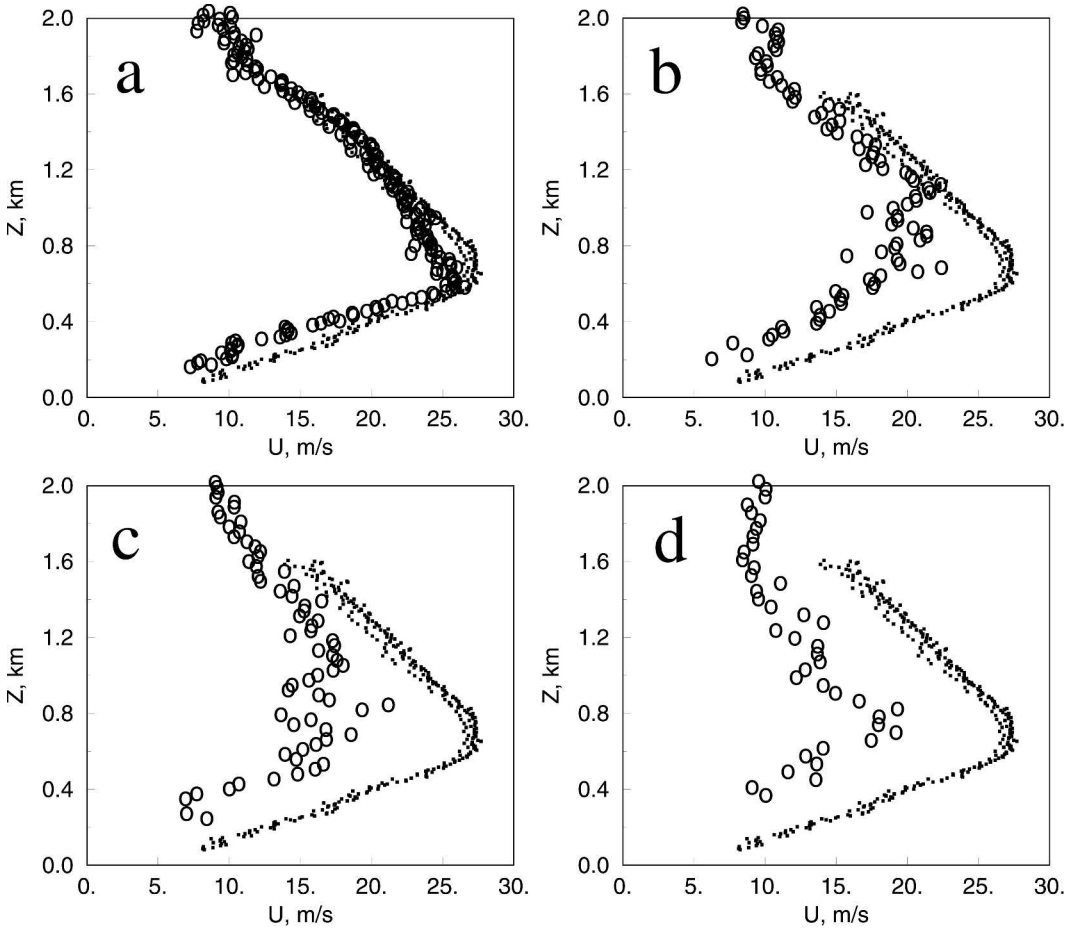

FIG. 14. VAD wind profiles from Cimarron radar near 0700 UTC 16 Jun 2000. Plotted open circles are profiles obtained from (a) 4°, (b) 8°, (c) 10°, and (d) 16°. Plotted dots are the profile obtained at 2° tilt.

were largely eliminated when wind profiles were obtained from scans at tilt angles of 1°–2°. For the 0.5° WSR-88D VAD wind profile, aggressively using spectral width information to filter the data produced a much more accurate wind profile. However, this was achieved at the expense of an increase in noise in the VAD due to much of the data being removed by filtering. With careful radar siting, or possibly more sophisticated ground clutter filtering, higher tilt angles could be used, with a consequent increase in vertical resolution and accuracy of the derived winds.

Acknowledgments. The authors gratefully acknowledge the assistance of Dusan Zrnić, for access to the Cimarron radar, and Josh Wurman, for access to the DOW3 radar. WSR-88D data were obtained from NCDC, and archived data for the S-Pol radar were obtained from NCAR. This research was supported by the Coastal Meteorological Research Program (CMRP) under Grant N00014-96-1-1112 from the U.S. Department of Defense (Navy), by the Center for the Analysis and Prediction of Storms (CAPS) under Grant ATM91-20009 from the National Science Foundation (NSF), by the NSF IHOP program under NSF Grant ATM01-29892, and by the University of Oklahoma. This research was also supported in part by the Engineering Research Centers Program of the National Science Foundation under NSF Award 0313747. Any opinions, findings, conclusions, or recommendations expressed in this study are those of the authors and do not necessarily reflect those of the National Science Foundation.

REFERENCES

Battan, L. J., 1973: *Radar Observations of the Atmosphere*. University of Chicago Press, 324 pp.

Browning, K. A., and H. Wexler, 1968: The determination of kinematic properties of a wind field using a Doppler radar. *J. Appl. Meteor.,* **7,** 105–113.

Doviak, R. J., and D. S. Zrnić, 1985: Siting of Doppler weather

radars to shield ground targets. *IEEE Trans. Antennas Propag.,* **33,** 685–689.

Klazura, G. E., and D. A. Imy, 1993: A description of the initial set of analysis products available from the NEXRAD WSR-88D system. *Bull. Amer. Meteor. Soc.,* **74,** 1293–1311.

Lhermitte, R. M., and D. Atlas, 1961: Precipitation motion by pulse Doppler radar. Preprints, *Ninth Weather Radar Conf.,* Kansas City, MO, Amer. Meteor. Soc., 218–223.

Martin, W. J., 2003: Measurements and modeling of the Great Plains low-level jet. Ph.D. dissertation, University of Oklahoma, 243 pp. [Available from University Microfilms, P.O. Box 1346, Ann Arbor, MI 48106-1346.]

OFCM, 1990: Doppler radar theory and meteorology. Part B, Doppler radar meteorological observations. Federal Meteorological Handbook 11, FCM-H11B-1990, Office of the Federal Coordinator for Meteorological Services and Supporting Research, 212 pp.

——, 1991: WSR-88D products and algorithms. Part C, Doppler radar meteorological observations. Federal Meteorological Handbook 11, FCM-H11C-1991, Office of the Federal Coordinator for Meteorological Services and Supporting Research, 210 pp.

Sherman, J. W., 1970: Aperture–antenna analysis. *Radar Handbook*, M. I. Skolnik, Ed., McGraw-Hill, 9-9–9-21.

Wilson, J. W., T. M. Weckwerth, J. Vivekanandan, R. M. Wakimoto, and R. W. Russell, 1994: Boundary layer clear-air radar echoes: Origin of echoes and accuracy of derived winds. *J. Atmos. Oceanic Technol.,* **11,** 1184–1206.

Wurman, J., J. Straka, E. Rasmussen, M. Randall, and A. Zahrai, 1997: Design and deployment of a portable, pencil-beam, pulsed 3-cm Doppler radar. *J. Atmos. Oceanic Technol.,* **14,** 1502–1512.

Zahrai, A., and D. S. Zrnić, 1993: The 10-cm wavelength polarimetric weather radar at NOAA's National Severe Storms Laboratory. *J. Atmos. Oceanic Technol.,* **10,** 649–662.